RESEARCH ARTICLE | MAY 08 2025

Ab initio phase diagrams of binary alloys in the low solute concentration limit

Shambhu Bhandari Sharma ; Shailesh Mehta; Dario Alfè

J. Chem. Phys. 162, 184502 (2025)
https://doi.org/10.1063/5.0264856

The Journal of Chemical Physics ARTICLE pubs.aip.org/aip/jcp

Ab initio phase diagrams of binary alloys in the low solute concentration limit

Cite as: J. Chem. Phys. 162, 184502 (2025); doi: 10.1063/5.0264856
Submitted: 12 February 2025 • Accepted: 21 April 2025 •
Published Online: 8 May 2025

Shambhu Bhandari Sharma,[1,a)] Shailesh Mehta,[2] and Dario Alfè[1,3,4]

AFFILIATIONS

[1] Department of Earth Sciences, University College London, Gower Street, London WC1E 6BT, United Kingdom
[2] AWE Nuclear Security Technologies, Aldermaston, Reading, Berkshire RG7 4PR, United Kingdom
[3] London Centre for Nanotechnology, University College London, London WC1E 6BT, United Kingdom
[4] Dipartimento di Fisica Ettore Pancini, Università di Napoli Federico II, Monte S. Angelo, I-80126 Napoli, Italy

[a)] **Author to whom correspondence should be addressed:** shambhu.sharma.22@ucl.ac.uk

ABSTRACT

Phase diagrams are crucial to the design of new materials, to understand their phase stability and metastability under different thermodynamic conditions, such as composition, temperature, and pressure. Here, we use an *ab initio* approach to study the phase diagram of a binary alloy within the low concentration limit of a solute. Using the *ab initio* molecular dynamics calculations based on density functional theory, we estimate the solute partitioning ratios in solid–liquid phase equilibria. The chemical potential difference between the solvent and solute atoms in both solid and liquid phases is calculated using thermodynamic integration. As an illustration of the techniques, we have applied this method to reproduce the phase diagram of the Al–Mg alloy at zero pressure. We also compute the *ab initio* solid–liquid coexistence curve of pure Al by applying the phase-coexistence method with the free energy correction technique. The calculated results are in close agreement with the experiment, demonstrating the reliability of the models.

I. INTRODUCTION

Phase diagrams are powerful analytical tools used in various scientific fields, including mineralogy, planetary sciences, materials science, and engineering. They provide a way to visualize how different phases of a material coexist under varying conditions. The prediction, determination, and validation of phase diagrams for alloys have a long history.[1] The inductive approach, based on phenomenological and semi-phenomenological models, has been widely employed to interpolate and extrapolate the experimental data to construct a comprehensive phase diagram. However, under extreme conditions, for example, relevant to planetary cores, where experimental data are unavailable, it would be useful to resort to a theoretical approach if this is proven reliably predictive.

Thanks to the steadily rising computational power and improvements in numerical algorithms, it is now possible to employ quantum mechanical *ab initio* molecular dynamics (AIMD) simulations to evaluate the chemical potential of elements in both solid and liquid phases.[2] AIMD simulations based on density functional theory (DFT) have been proven to be highly accurate over a wide range of pressures and temperatures.[3–5]

To understand the solid–liquid phase equilibria of a multicomponent system, it is necessary to evaluate the chemical potentials of all its constituents. Since these can be defined as free energy differences, it is possible to compute them using, for example, thermodynamic integration approaches.[5–7] For one-component systems, such as pure metals, thermodynamic integration has been extremely successful in determining the free energy and hence the *ab initio* solid–liquid coexistence curve up to high pressures.[8–11]

The phase diagram of binary alloys, for instance, Al–Mg alloy, has been studied using experimental[12] and theoretical (classical) models[13] under ambient pressure conditions. Al–Mg is an important class of non-heat-treatable binary alloy,[14] deployed experimentally, and has several industrial applications. To understand the phases, compositions, and thermodynamic stability as a function of temperature and concentration, it is fundamental to explore their phase

diagram, using *ab initio* calculations, not only to complement the experiments but also to predict the phases or metastable states, especially at high pressures/temperature, that are not easily observed in the experiment.

In this work, we aim to develop a model to compute the *ab initio* phase diagram of binary alloys in the small concentration limit of solute. An earlier approach for computing *ab initio* chemical potentials of solids and liquids was introduced to study the partitioning of impurities under the earth's core condition.[5] Here, we revisit the method with the aim to provide a simpler approach, which can be applied with little or no modifications to existing *ab initio* codes, which is a significant advantage for a more widely takeover of the techniques. The method becomes formally exact in the limit of small concentrations. As a demonstration of the techniques, we will determine the phase diagram of the Al–Mg alloy at a low concentration of Mg. Before taking the alloy, we will first present a calculation of the *ab initio* melting curve of pure Al, comparing it with experiments and previous first-principles results. The approach we use is based on the coexistence of phases, performed with an empirical potential fitted onto *ab initio* data, followed by free energy corrections from the empirical model to the full *ab initio* system to provide the melting curve in the pressure region ≈ 0–150 GPa.

The structure of this paper is as follows: In Sec. I, we present the theoretical basis and computational details implemented in the phase coexistence method and free energy correction and the details of the technique to compute the chemical potential differences. In Sec. III, we begin by presenting the calculation results for the melting curve of pure Al, then discuss the strategy of our model and present the results for room pressure *ab initio* phase diagram of an Al–Mg alloy, and compare our results with the available literature. The concluding remarks of this work are given in Sec. IV.

II. THEORETICAL AND COMPUTATIONAL DETAILS

A. Coexistence simulation and free energy correction

We choose a reference model based on an embedded-atom model (EAM)[15] fitted to DFT results. The total energy function of the EAM, U_{ref}, is

$$U_{\mathrm{ref}} = \frac{1}{2}\sum_{i\neq j}\varepsilon\left(\frac{a}{r_{ij}}\right)^{n} - \varepsilon C\sum_{i}\left[\sum_{(j\neq i)}\left(\frac{a}{r_{ij}}\right)^{m}\right]^{1/2}, \tag{1}$$

where ε, a, C, n, and m are fitting parameters—the separation of atoms at position r_i and r_j is denoted by r_{ij}. This potential is cut and shifted at 5.5 Å to remove discontinuity in the forces in all the classical molecular dynamics (CMD) simulations.

The shift in melting temperature from the reference potential to the *ab initio* system, ΔT, to first order, can be obtained from the Gibbs free energy difference between the *ab initio* system and the EAM, in solid and liquid. We call this difference ΔG^{ls}. The shift is given by

$$\Delta T \approx \frac{\Delta G^{ls}\left(T_m^{\mathrm{ref}}\right)}{S_{\mathrm{ref}}^{ls}}, \tag{2}$$

where S_{ref}^{ls} is the entropy of melting and T_m^{ref} is the classical melting temperature obtained from the coexistence simulation.

To compute ΔG^{ls}, we first calculate the change in the Helmholtz free energy ΔF. We do this by using a perturbative expansion, which relies on sampling the configuration space only with the reference model,

$$\Delta F \approx \langle \Delta U\rangle_{\mathrm{ref}} - \frac{1}{2k_{\mathrm{B}}T}\left\langle \delta\Delta U^{2}\right\rangle_{\mathrm{ref}}, \tag{3}$$

where $\langle\cdot\rangle_{\mathrm{ref}}$ denotes the thermal average evaluated in the reference potential ensemble, k_B is the Boltzmann constant, $\Delta U = U_{\mathrm{DFT}} - U_{\mathrm{ref}}$, and $\delta\Delta U = \Delta U - \langle\Delta U\rangle_{\mathrm{ref}}$. Here, U_{DFT} and U_{ref} are the total energy function of the *ab initio* system (DFT) and the reference system (EAM), respectively.

To obtain ΔG, we expand it in terms of the change of pressure as the potential energy function is changed from that of the EAM to the DFT one, Δp. It is easy to show that the zero-order term of the expansion is equal to ΔF, the first order term is zero, and the second order term is given by

$$\Delta G \approx \Delta F - \frac{1}{2}\frac{V\Delta p^{2}}{K_T}, \tag{4}$$

where K_T is the isothermal bulk modulus. Equations (2)–(4) are good approximations to the exact calculations, and this approximation is reliable only in the limit of U_{ref} being close enough to U_{DFT}, with small fluctuations, to support the perturbative approach; for full details, see Ref. 16.

B. The chemical potential and the phase diagram

For a two-component mixture, a binary A–X alloy, where A is the solvent and X is the solute, the solid–liquid phase equilibrium at the melting temperature T_m and pressure p requires

$$\mu_{\mathrm{X}}^{l}\left(p, T_m, c_{\mathrm{X}}^{l}\right) = \mu_{\mathrm{X}}^{s}\left(p, T_m, c_{\mathrm{X}}^{s}\right), \tag{5}$$

$$\mu_{\mathrm{A}}^{l}\left(p, T_m, c_{\mathrm{X}}^{l}\right) = \mu_{\mathrm{A}}^{s}\left(p, T_m, c_{\mathrm{X}}^{s}\right), \tag{6}$$

where μ_{X} and μ_{A} are the chemical potentials of the X and A species, respectively, and c_{X} is the mole fraction of X, with the superscripts l and s denoting liquid and solid, respectively.

In the low-concentration limit of $c_{\mathrm{X}} \to 0$, μ_{X} diverges logarithmically, and we can rewrite it as

$$\mu_{\mathrm{X}}(p, T_m, c_{\mathrm{X}}) = k_B T_m \ln(c_{\mathrm{X}}) + \bar{\mu}_{\mathrm{X}}(p, T_m, c_{\mathrm{X}}), \tag{7}$$

where $\bar{\mu}_{\mathrm{X}}(p, T_m, c_{\mathrm{X}})$ accounts for the behavior of the chemical potential that remains finite and well-defined even $c_{\mathrm{X}} \to 0$.

Using Eq. (5) in Eq. (7), we obtain the ratio of the concentrations between the two phases,

$$c_{\mathrm{X}}^{s}/c_{\mathrm{X}}^{l} = \exp\left[\left(\bar{\mu}_{\mathrm{X}}^{l} - \bar{\mu}_{\mathrm{X}}^{s}\right)/k_B T_m\right]. \tag{8}$$

The variation of $\bar{\mu}_{\mathrm{X}}(p, T_m, c_{\mathrm{X}})$ with c_{X} to the lowest order is expanded as[5]

$$\bar{\mu}_{\mathrm{X}}(p, T_m, c_{\mathrm{X}}) = \mu_{\mathrm{X}}^{\dagger}(p, T_m) + \lambda_{\mathrm{X}}(p, T_m)c_{\mathrm{X}} + O\left(c_{\mathrm{X}}^{2}\right). \tag{9}$$

Here, the term $\mu_{\mathrm{X}}^{\dagger}(p, T_m)$ indicates the excess chemical potential of solute in the limit of zero concentration and λ_{X} is a coefficient that quantifies the linear dependence of $\bar{\mu}_{\mathrm{X}}(p, T_m, c_{\mathrm{X}})$ on c_{X}.

Now, neglecting the term $O(c_X^2)$ systematically, Eq. (8) becomes

$$c_X^s/c_X^l = \exp\left[\left(\mu_X^{\dagger l} - \mu_X^{\dagger s} + \lambda_X^l c_X^l - \lambda_X^s c_X^s\right)/k_B T_m\right]. \quad (10)$$

We further approximate the condition of solute in the limit of infinite dilution, $c_X \approx 0$, and neglect the linear order term, which gives

$$c_X^s/c_X^l = \exp\left[\left(\mu_X^{\dagger l} - \mu_X^{\dagger s}\right)/k_B T_m\right]. \quad (11)$$

To obtain the change in μ_A in response to a change in composition c_X, we use the Gibbs–Duhem equation,

$$c_A d\mu_A + c_X d\mu_X = 0, \quad (12)$$

which gives

$$\mu_A(p, T_m, c_X) = \mu_A^0(p, T_m) + (k_B T_m + \lambda_X(p, T_m)) \ln(1 - c_X) \times \lambda_X(p, T_m) c_X + O(c_X^2), \quad (13)$$

where $\mu_A^0(p, T_m)$ is the chemical potential of pure A and T_m is the equilibrium temperature. We use $c_A = 1 - c_X$. By neglecting second order terms in c_X, we obtain

$$\mu_A(p, T_m, c_X) = \mu_A^0(p, T_m) - k_B T_m c_X + O(c_X^2). \quad (14)$$

We expand $\mu_A^0(p, T_m)$ to linear order as a function of the difference $T_m - T_m^0$, where T_m^0 is the melting temperature of pure solvent A,

$$\mu_A^0(p, T_m) \sim \mu_A^0(p, T_m^0) + \left(\frac{\partial \mu_A^0}{\partial T_m}\right)_{T_m = T_m^0} (T_m - T_m^0). \quad (15)$$

Using Eqs. (14) and (15) in Eq. (6), we obtain

$$\mu_A^{0l}(p, T_m^0) - k_B T_m c_X^l + (T_m - T_m^0)\left(\frac{\partial \mu_A^{0l}}{\partial T}\right)_{T=T_m^0} = \mu_A^{0s}(p, T_m^0) - k_B T_m c_X^s + (T_m - T_m^0)\left(\frac{\partial \mu_A^{0s}}{\partial T}\right)_{T=T_m^0}. \quad (16)$$

Since $\mu_A^{0s} = \mu_A^{0l}$, Eq. (16) reduces to

$$k_B T_m c_X^l + (T_m - T_m^0) s_A^{0l} = k_B T_m c_X^s + (T_m - T_m^0) s_A^{0s}, \quad (17)$$

where $s_A^0 = -\left(\frac{\partial \mu_A^{0l}}{\partial T}\right)_{T=T_m^0}$ denotes the entropy per atom of pure A at the melting temperature. Then, we obtain the shift of melting temperature as a function of c_X,

$$(T_m - T_m^0) = \frac{k_B T_m}{\Delta s_A^0}\left(c_X^s - c_X^l\right). \quad (18)$$

Note that the new equilibrium temperature T_m corresponds, in general, to two different concentrations in solid and liquid. The change in T_m in the liquid as a function of c_X^l is known as the *liquidus*, T_m^l, and that of T_m in the solid as a function of c_X^s is known as the *solidus*, T_m^s. Using Eq. (11) in Eq. (18), the liquidus and solidus temperatures are expressed as

$$T_m^l = T_m^0 + \frac{k_B T_m^l}{\Delta s_A^0}\left(\exp\left[\Delta\mu_X^{ls}/k_B T_m^l\right] - 1\right)c_X^l, \quad (19)$$

$$T_m^s = T_m^0 + \frac{k_B T_m^s}{\Delta s_A^0}\left(1 - \exp\left[-\Delta\mu_X^{ls}/k_B T_m^s\right]\right)c_X^s, \quad (20)$$

where $\Delta\mu_X^{ls} = \mu_X^{\dagger l} - \mu_X^{\dagger s}$ and Δs_A^0 denotes the entropy of fusion of the pure solvent A. Hence, we identify that T_m^0, $\Delta\mu_X^{ls}$, and Δs_A^0 are the thermodynamic quantities required to compute the phase diagram. Solving these transcendental equations (19) and (20) self-consistently, we can obtain the *ab initio* phase diagram of the binary A–X alloy.

C. Computational details

We have used the projector-augmented-wave method[17,18] as implemented in Vienna *Ab initio* Simulation Package (VASP)[19] to perform all DFT and AIMD calculations. The underlying exchange–correlation energy is treated by generalized gradient approximation of Perdew–Burke–Ernzerhof (PBE).[20] The core radii for Al and Mg are of 1.01 and 1.06 Å, respectively. A value of 312 eV is set for the cutoff energy, and k-points of Monkhorst–Pack[21] are used in Brillouin zone sampling. The finite-temperature formulation of DFT by Mermin (Ref. 22) is used to address the thermal excitation of electrons at high temperatures. The constant temperature in AIMD is achieved using a Nosé[23] thermostat.

III. RESULTS AND DISCUSSION

A. Solid–liquid coexistence curve of aluminum

As a starting point, we begin by computing the *ab initio* melting curve of pure Al, applying the solid–liquid phase coexistence and then free energy correction technique, following the procedure outlined in Ref. 16. We initiate the calculation by performing AIMD simulations within the canonical ensemble (NVT) at a pressure ≈0 GPa for the solid and ≈4 GPa for the liquid. From the trajectory of the AIMD simulations, we then extract 150 configurations and their corresponding pressure and energies. We utilize these extracted quantities to fit the EAM parameters. The value of the fitted parameters are $\varepsilon = 0.1267$ eV, $a = 3.1233$ Å, $C = 9.9748$, $n = 7.4197$, and $m = 3.4677$. For the high-pressure region, we retune the fitted parameters to $\varepsilon = 0.1138$ eV, $a = 3.0556$ Å, $C = 9.9749$, $n = 7.5452$, and $m = 3.5012$ by fitting with AIMD results at $p \approx 130$ GPa.

We create a large 10 × 10× 20 rectangular supercell box containing 8000 aluminum atoms and perform the CMD simulation under microcanonical conditions (NVE) for 300 ps and at a time step of 1 fs. The drift in the equation of motion is monitored by varying the simulation time step from 1 fs to 3 fs, and it is found that a time step of 1 fs gives the minimum drift less than 0.04 K/ps. Finally, the standard reblocking procedure[24] is used to inspect the error in melting temperature and found negligible (less than 5 K).

To calculate the free energy corrections between DFT and the EAM, we perform two independent CMD calculations using 500 Al

atoms for both solid and liquid in the canonical ensemble maintaining the melting conditions (p, T_m^{ref}) for 100 ps of the simulation period. We extract several (typically>50) statistically independent configurations and perform DFT total energy calculations using a k-grid sampling of Γ point, 2 × 2× 2, and 3 × 3× 3. We find that the value of ΔG^{ls} is converged at a 2 × 2× 2 k-grid with a precision <1 meV/atom when the number of configurations > 50 is used [Fig. 1(a)]. The *ab initio* melting curve, including the melting temperature and slope dT_m/dp = 65 K/GPa at $p \approx 0$ GPa, is in excellent agreement with previous *ab initio* calculations[25] and experiments[26,27,29–31] as depicted in Fig. 1(b).

B. Phase diagram of Al–Mg alloy

Moving beyond the one-component system, we develop a model for the *ab initio* phase diagram of a two-component alloy system $A - X$ (A = Al and X = Mg) based on chemical potential calculations of the mixing components using the thermodynamic integration technique. The chemical potential μ of a solute X in solid or liquid solvent A is either the Gibbs free energy change when an atom of X is introduced to the system at constant temperature T and pressure p or the change in Helmholtz free energy at constant T and volume V. It is convenient to convert solvent into solute, which gives the chemical potential difference $\mu_X - \mu_A$ for both solid and liquid phases at constant V. For two systems containing the same number of atoms, but having different total energy functions U_1 and U_0, the value of $\mu_X - \mu_A$ can be calculated using thermodynamic integration, computing the Helmholtz free energy difference $F_1 - F_0$. This provides the reversible work performed during the continuous transition from U_0 to U_1 at constant volume, expressed as

$$F_1 - F_0 = \int_0^1 d\lambda \langle U_1 - U_0 \rangle_\lambda, \tag{21}$$

where $\langle \ldots \rangle_\lambda$ denotes the equilibrium ensemble average for the system with the hybrid energy function $U_\lambda = (1-\lambda)U_0 + \lambda U_1$. This technique has been used in many DFT studies.[5,11,32,33] If U_0 and U_1 are close, using the perturbative approach, we can calculate the free energy difference from the two ends at $\lambda = 0$ and $\lambda = 1$,

$$F_1 - F_0 \approx \langle U_1 - U_0 \rangle_{\lambda=0} - \frac{1}{2k_B T} \langle \delta \Delta U^2 \rangle_{\lambda=0} \tag{22}$$

and

$$F_0 - F_1 \approx \langle U_0 - U_1 \rangle_{\lambda=1} - \frac{1}{2k_B T} \langle \delta \Delta U^2 \rangle_{\lambda=1}. \tag{23}$$

To determine the phase diagram of the Al–Mg alloy at p = 0 GPa, we perform NVT AIMD calculations for both the pure Al system $\lambda = 0$ and the Al–Mg system (Al system with one atom substituted by Mg atom) $\lambda = 1$ in solid and liquid phases. We then extract a large number of independent configurations from their trajectories. From the pure Al configurations, corresponding to $\lambda = 0$, we compute both the pure Al energies, U_0, and the energies U_1 where one Al atom has been replaced with a Mg atom. From the Al–Mg configurations, generated with a system containing one Mg atom in place of an Al atom, and therefore corresponding to $\lambda = 1$, we compute once again both the pure Al energies, whereby the Mg atom has been replaced with an Al atom, and the Al–Mg energies.

The total energies of the pure Al system, U_0, and Al–Mg system, U_1, is calculated using DFT single-point calculations, and $\langle U_1 - U_0 \rangle_{\lambda=0}$ and $\langle U_1 - U_0 \rangle_{\lambda=1}$ are evaluated, together with the corresponding fluctuations. If the fluctuations are not too large (less than a few tens of meV/atom), we compute the change in free energy for both solid and liquid phases as

$$\Delta F = \frac{\langle \Delta U \rangle_{\lambda=0} + \langle \Delta U \rangle_{\lambda=1}}{2}. \tag{24}$$

If the fluctuations are larger, then we include the slope from the fluctuation to $\langle \Delta U \rangle_\lambda$ at the two end points $\lambda = 0$ and $\lambda = 1$, for both solid and liquid, we join the two linear relations at their intersection point, which lies between 0 and 1. We then calculate the area under the resulting piecewise linear curve, which provides a more accurate value of $\Delta \mu^{ls}_{\mathrm{Mg}}$.

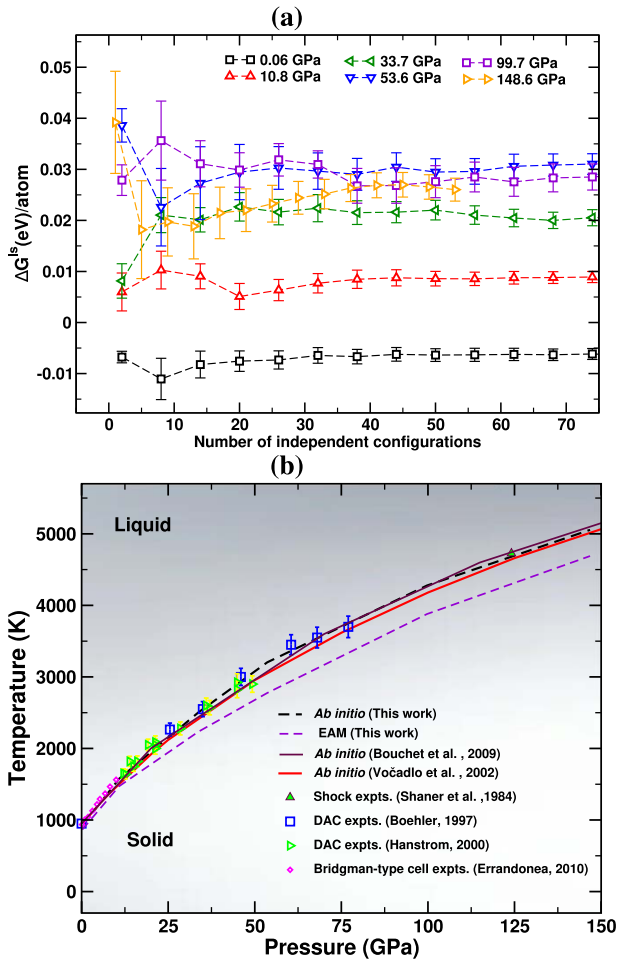

FIG. 1. (a) Free energy differences between solid and liquid, including error bars, with respect to the number of independent configurations at different pressures and (b) comparison of the calculated *ab initio* melting curve of Al with the available literature.[4,25–28]

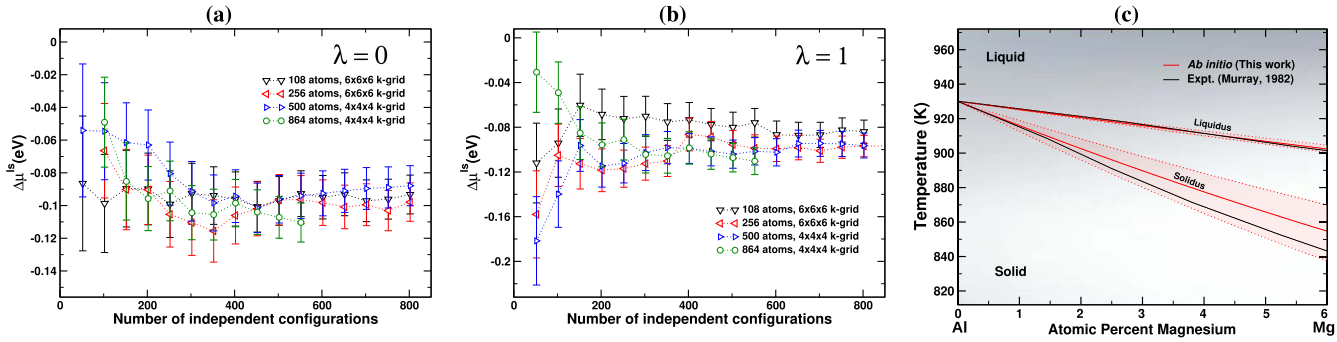

FIG. 2. [(a) and (b)] Chemical potential differences of Mg atom between solid and liquid $\Delta\mu^{ls}_{Mg}$ with error bars, using different numbers of independent configurations, numbers of atoms, and k-points for $\lambda = 0$ and $\lambda = 1$, respectively. (c) Calculated *ab initio* phase diagram of Al–Mg alloy up to six atomic percentage of Mg and the experimental result.[12] The shaded red region between the dotted lines represents the error range, based on the one sigma error bars from the computed chemical potential.

In addition, the entropy of melting of pure Al at pressure p and temperature T is readily calculated by using the energies and volumes of solid and liquid,

$$\Delta s^0_{Al} = \frac{E^l - E^s + p(V^l - V^s)}{T}. \quad (25)$$

The AIMD simulations, under the canonical ensemble, are performed for both solid and liquid phases using different numbers of atoms over a simulation period up to 40 ps to produce $p = 0$ GPa at T = 920K. We use 2 × 2× 2 k-mesh sampling for a supercell containing 108, 256, and 500 Al atoms, while Γ-point sampling for a larger system with 864 atoms. The total energy single-point calculation is performed using symmetric k-points up to 6 × 6× 6. Interestingly, we found that convergence with respect to k-point sampling is much faster if we use grids reduced to only the points of the irreducible Brillouin zone of the perfect crystal. This is explained by the fact that both solid and liquid, when averaged over hundreds of configurations, have approximately the same full cubic symmetry. To investigate the convergence, we calculate $\Delta\mu^{ls}_{Mg}$ using Eqs. (22) and (23), varying the numbers of atoms, k-points, and statistically independent configuration, as presented in Fig. 2(a) for $\lambda = 0$ and in Fig. 2(b) for $\lambda = 1$. It is clear that a supercell containing 256 atoms with a 6 × 6× 6 symmetric k-grid with independent configurations > 400 gives the converged value of $\Delta\mu^{ls}_{Mg}$.

Using the techniques explained above, the values of $\Delta\mu^{ls}_{Mg}$ and Δs^0_{Al} are determined to be −0.088 ± 0.012 eV/atom and 1.35 kB, respectively, at zero pressure. From Eqs. (19) and (20), we determine the solidus and liquidus and hence the *ab initio* phase diagram of Al–Mg up to six atomic percentage of Mg, as shown in Fig. 2(c). Here, we arbitrarily cut at 6% because our method is, as described before, only effective in the zero concentration limit, and therefore, errors become larger at larger concentrations. The calculated solidus and liquidus lines are in good agreement with the experiment, within a one-sigma error band region.

IV. CONCLUSION

We have shown that the phase-coexistence method with free energy correction is an effective technique for calculating the *ab initio* solid–liquid coexistence curve for a single-component system, as demonstrated by applying this method to pure aluminum. The success of this method depends heavily on the quality of fitting the reference potential with DFT.

Most importantly, we have introduced a concise model to compute the *ab initio* phase diagram of the two-component alloy A–X system (here A = Al; X = Mg), which is based on calculating the chemical potential difference of solute X in solvent A, using the thermodynamic integration technique. The phase diagram for Al–Mg alloys, calculated using this model at zero pressure and within a small concentration limit of Mg, is in fair agreement with the experimental results.

The method presented to calculate the *ab initio* phase diagram of binary alloy is designed to be widely applicable to any two-component alloy systems where the focus is on the limit of small concentration. The primary advantages of the method are its generality and ease of implementation. It is easy to implement using general purpose DFT codes, without requiring in depth modifications of the codes themselves. As a result, one can build workflows easily applicable to a large variety of systems to calculate the phase diagram up to high pressures, which is unique compared to other available methods.

ACKNOWLEDGMENTS

We acknowledge the support of AWE Nuclear Security Technologies and the HPC facility at UCL. This work also used the ARCHER2 UK National Supercomputing Service (https://www.archer2.ac.uk), under the Mineral Consortium allocation.

AUTHOR DECLARATIONS

Conflict of Interest

The authors have no conflicts to disclose.

Author Contributions

Shambhu Bhandari Sharma: Investigation (equal); Writing – original draft (equal). **Shailesh Mehta**: Funding acquisition (supporting). **Dario Alfè**: Supervision (equal).

DATA AVAILABILITY

The data that support the findings of this study are available from the corresponding author upon reasonable request.

REFERENCES

[1] J. Schön and M. Jansen, Int. J. Mater. Res. **100**, 135 (2009).
[2] P. Y. Chew and A. Reinhardt, J. Chem. Phys. **158**, 030902 (2023).
[3] X. Wang, M. Yang, X. Gai, Y. Sun, B. Cao, J. Chen, M. Liang, F. Tian, and L. Li, J. Mol. Liq. **395**, 123924 (2024).
[4] J. Bouchet, F. Bottin, G. Jomard, and G. Zérah, Phys. Rev. B **80**, 094102 (2009).
[5] D. Alfè, M. Gillan, and G. Price, J. Chem. Phys. **116**, 7127 (2002).
[6] F. Della Pia and D. Alfè, Phys. Rev. B **105**, 134109 (2022).
[7] J. Deng and L. Stixrude, Earth Planet. Sci. Lett. **562**, 116873 (2021).
[8] L. Shulenburger, M. P. Desjarlais, and T. R. Mattsson, Phys. Rev. B **90**, 140104 (2014).
[9] F. Colonna, J. H. Los, A. Fasolino, and E. J. Meijer, Phys. Rev. B **80**, 134103 (2009).
[10] M. Pozzo and D. Alfè, Phys. Rev. B **88**, 024111 (2013).
[11] L. Vočadlo, D. Alfè, G. Price, and M. Gillan, J. Chem. Phys. **120**, 2872 (2004).
[12] J. L. Murray, J. Phase Equilib. **3**, 60 (1982).
[13] M. i. Mendelev, M. Asta, M. j. Rahman, and J. j. Hoyt, Philos. Mag. **89**, 3269 (2009).
[14] M. P. Liu, H. J. Roven, M. Y. Murashkin, R. Z. Valiev, A. Kilmametov, Z. Zhang, and Y. Yu, J. Mater. Sci. **48**, 4681 (2013).
[15] M. S. Daw and M. I. Baskes, Phys. Rev. Lett. **50**, 1285 (1983).
[16] D. Alfè, M. Gillan, and G. Price, J. Chem. Phys. **116**, 6170 (2002).
[17] P. E. Blöchl, Phys. Rev. B **50**, 17953 (1994).
[18] G. Kresse and D. Joubert, Phys. Rev. B **59**, 1758 (1999).
[19] G. Kresse and J. Furthmüller, Phys. Rev. B **54**, 11169 (1996).
[20] J. P. Perdew, K. Burke, and M. Ernzerhof, Phys. Rev. Lett. **77**, 3865 (1996).
[21] H. J. Monkhorst and J. D. Pack, Phys. Rev. B **13**, 5188 (1976).
[22] N. D. Mermin, Phys. Rev. **137**, A1441 (1965).
[23] S. Nosé, Mol. Phys. **52**, 255 (1984).
[24] M. P. Allen and D. J. Tildesley, *Computer Simulation of Liquids* (Oxford Science, London, 1987).
[25] L. Vočadlo and D. Alfè, Phys. Rev. B **65**, 214105 (2002).
[26] R. Boehler and M. Ross, Earth Planet. Sci. Lett. **153**, 223 (1997).
[27] A. Hänström and P. Lazor, J. Alloys Compd. **305**, 209 (2000).
[28] D. Errandonea, J. Appl. Phys. **108**, 033517 (2010).
[29] A. Jayaraman, W. Klement, Jr, R. c. Newton, and G. c. Kennedy, J. Phys. Chem. Solids **24**, 7 (1963).
[30] J. W. Shaner, J. M. Brown, and R. G. McQueen, in *High Pressure in Science and Technology*, edited by C. Homan, R. C. MacCrone, and E. Whalley (Elsevier, North Holland, Amsterdam, 1984), p. 137.
[31] J. F. Cannon, J. Phys. Chem. Ref. Data **3**, 781 (1974).
[32] T. Taniuchi and T. Tsuchiya, J. Phys.: Condens. Matter **30**, 114003 (2018).
[33] E. Smargiassi and P. A. Madden, Phys. Rev. B **51**, 117 (1995).